Self assembled fullerene walls in di-mesogenic-C60 materials

Silvia Orlandi,[a] **Luca Muccioli,**[a] **Matteo Ricci,**[a] **and Claudio Zannoni**[a]

We present a Monte Carlo simulation study of the phase behaviour and molecular organization of fullerene-based compounds, formed by a central fullerene with two mesogenic groups attached at its sides, that we describe with a generalized Gay-Berne model with flexible spacers. We consider two cases with identical substituents, either rod-like or disc-like, and investigate the thermotropic phases they form, focusing on the microsegregation and spatial organization of the fullerene and mesogen moieties, also in view of the potential interest for organic solar cells. The simulations produce, for these phases, equilibrium configurations with partial or complete two-dimensional segregation of C60 from mesogenic moieties. The predicted phase organisations seem very promising in terms of optimization of charge and energy transport properties.

I Introduction

Fullerene based materials have been shown to provide an important route towards producing efficient organic electronic devices, such as field effect transistors [1,2,3] and, in particular, photovoltaic cells [4,5,6]. The emphasis on fullerenes stems from their belonging to the relatively small number of n-type semiconductors and from other appealing characteristics for charge transfer, like having, in the terminology of Marcus theory, a low reorganization energy [7] as well as showing a large increase in photoconductivity when illuminated [4,8].

In the simplest picture of a fullerene-based solar cell functioning, a suitable organic moiety (most often a conjugated polymer or a phthalocyanine) is photoexcited and acts as an electron donor towards a fullerene derivative acceptor [7,9] at their interface (heterojunction), where charge separation takes place. The device performance is related, amongst other, to the morphology of the conjugated polymer-C60 blend [10,11], that, ideally, should be formed by contiguous microstructures where the separated charges can be effectively transported in a percolating network towards the electrodes, rather than recombining. Among the attempts at optimizing efficiency through morphology control, different device architectures have been put forward, ranging from thin film double [12] and multiple layers [13], to polymer-fullerene bulk heterojunctions [14] or laminated layers [15].

On the negative side, fullerenes have a strong tendency to attract each other, and their intermolecular potential has an estimated well depth of about 30 kJ/mol [16]. Since this in turn leads to low solubility, easy aggregation and phase separation from the blend, either more soluble derivatives [17] or compounds where the fullerene is directly linked to the organic polymer have been prepared and actively investigated [18,19]. In this line of work fullerene – mesogen compounds, synthesized relatively recently [8,20,21,22,23], present, at least in principle, some innovative possibilities of (i) intrinsic separation of the p- and n- type regions as well as of (ii) structuring of the conjugated organic parts so as to favour π-stacking while (iii) conserving to some extent the fluidity and the defect self-annealing capability typical of liquid crystals, avoiding the grain boundary limitations to carrier transport characteristic of crystalline materials [24,25]. With these general principles in mind it seems useful to try and provide some elements of molecular design for these new materials. Although some theoretical foresights in this direction have been recently published, based on lattice models and statistical mechanics density functional theory [26,27], much remains to be done to predict the phase types and molecular organizations obtainable from a given fullerene-mesogen hybrid compound. Unfortunately this task does not lend itself to simple physical intuition, as it is obvious from the very unlikely nature of a mesogenic compound containing a relatively large and apparently disruptive spherical unit.

In a first attempt to employ molecular level computer simulations in this respect, we have shown that a simple model mesogen formed by a central fullerene (F) with two rod like mesogenic units attached at the sides (R-F-R) could form nematic and smectic phases, at least for certain mesogenic aspect ratios [28].

However the model in [28] makes the particularly strong assumption of the mesogens being rigidly connected to the central C60 and this limits its realism. Indeed practically all hybrid compounds synthesized until now have the mesogens connected by flexible spacers (see e.g. Fig. 1) and, even more importantly, the flexible spacers seem essential in order to accommodate the bulky fullerene and obtain a variety of locally heterogeneous phase organizations.

In this paper we propose a generalization of our previous model where the C60 is connected to each mesogenic moiety by a spacer, mimicked by a flexible spring and we study, with Monte Carlo (MC) simulations, the phase behavior and molecular organization for two families of compounds

where C60 is located at the central position with two rod-like (R-F-R) or disc-like (D-F-D) mesogenic units attached laterally (Fig. 2).

a)

b)
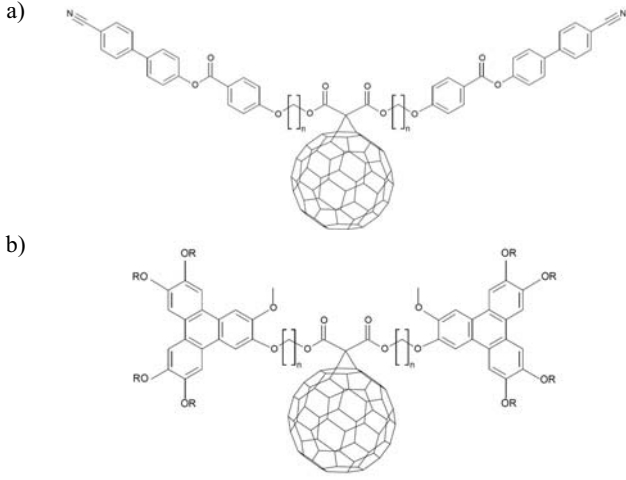
Fig. 1 Examples of molecular structures of mesogenic fullerene derivatives of the R-F-R (a) and D-F-D (b) type [29,39].

While this work is aimed at understanding trends, rather than attempting to reproduce experimental data, our model provides a good starting point for further refinements aimed at constructing more detailed and specific models.

II Model and computational details

We set out to implement the essential molecular characteristics of two classes of compounds, where the mesogens attached to the fullerene are respectively calamitic or discotic (see Fig. 1). Here we have employed a three-site flexible model with a central sphere representing the C60 unit and two equivalent uniaxial Gay-Berne (GB) ellipsoids [30,31], either prolate or oblate, representing the lateral mesogenic moieties (Fig. 2).

a)

b)
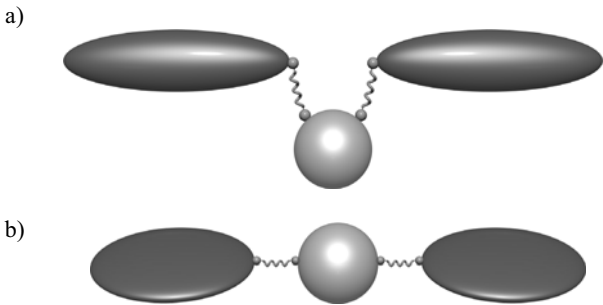
Fig. 2 Sketch of the proposed models for R-F-R (a) and D-F-D (b) derivatives.

Each ellipsoidal site is connected to the fullerene sphere by a flexible spring [32,33]. We assume the bonding interaction sites to be placed on the surface of the sphere and of the ellipsoids, and that the bonds cannot break during the simulation, but only stretch and bend. These last terms consist of harmonic contributions depending on the separation $s_{ij} = |\mathbf{p}_j - \mathbf{p}_i|$, and angles $\theta_{ij} = \cos^{-1}(\mathbf{u}_i \cdot \mathbf{u}_j)$ between two linked bonding sites:

$$U_{bond} = k_s(s_{ij} - s_{eq})^2 + k_\theta(\theta_{ij} - \theta_{eq})^2 \tag{1}$$

where $\mathbf{p}$ and $\mathbf{u}$ are the positions and the orientations of the bonding sites, s_{eq} and θ_{eq} the equilibrium spacer length and bend angle, and k_s, k_θ the stiffness parameters of the spacer. For both rod and disc mesogenic units, we have used the same spacer, with bending harmonic constant $k_\theta = 200$ rad^{-2}, bond angle $\theta_{eq} = 180°$, stretching harmonic constant $k_s = 500$ and slightly different length ($s_{eq} = 0.1$ and 0.2 for rods and discs [33] respectively).

Table 1 Dimensions $\sigma_\perp, \sigma_\parallel$ (in σ_0 units), energy well widths $\varepsilon_\perp, \varepsilon_\parallel$ (ε_0 units) of mesogenic (R) and fullerenic (F) moieties, positions p_x, p_y, p_z (σ_0 units) and orientations u_x, u_y, u_z of their binding sites with respect to the GB site center ($\sigma_0 = 10$ Å, $\varepsilon_0 = 1.4$ kcal/mol). GB exponents $\mu = 1$, $v = 3$, flexible spacer parameters $s_{eq} = 0.1\sigma_0$, $\theta_{eq} = 180°$, $k_s = 500$, $k_\theta = 200$ rad^{-2}.

S	$\sigma_\perp$	$\sigma_\parallel$	σ_c	$\varepsilon_\perp$	$\varepsilon_\parallel$	n_b	p_x	p_y	p_z	u_x	u_y	u_z
R	0.7	2.6	0.7	1.0	0.2	1	0.0	0.0	+1.3	−0.866	0.	−0.5
R	0.7	2.6	0.7	1.0	0.2	1	0.0	0.0	−1.3	−0.866	0.	−0.5
F	0.95	0.95	0.45	4.5	4.5	2	0.23	0.0	±0.414	0.866	0.	±0.5

Table 2 Dimensions $\sigma_\perp, \sigma_\parallel$ (σ_0 units), energy well widths $\varepsilon_\perp, \varepsilon_\parallel$ (ε_0 units) of mesogenic (D) and fullerenic (F) moieties, positions p_x, p_y, p_z (σ_0 units) and orientations u_x, u_y, u_z of their binding sites with respect to the GB site center ($\sigma_0 = 10$ Å, $\varepsilon_0 = 1.4$ kcal/mol). GB exponents $\mu = 1$, $v = 0$, flexible spacer parameters $s_{eq} = 0.2\sigma_0$, $\theta_{eq} = 180°$, $k_s = 500$, $k_\theta = 200$ rad^{-2}.

S	$\sigma_\perp$	$\sigma_\parallel$	σ_c	$\varepsilon_\perp$	$\varepsilon_\parallel$	n_b	p_x	p_y	p_z	u_x	u_y	u_z
D	1.925	0.375	0.375	0.3	2.0	1	-.9625	0.0	0.0	-1.	0.0	0.0
D	1.925	0.375	0.375	0.3	2.0	1	+.9625	0.0	0.0	-1.	0.0	0.0
F	0.95	0.95	0.45	4.5	4.5	2	±0.475	0.0	0.0	0.	0.0	±1.0

Each GB site interacts via a potential that is a special case of the expression previously developed for dissimilar Gay-Berne biaxial particles [34]:

$$U_{AB}(\omega_1, \omega_2, \mathbf{r}_{AB}) = 4\varepsilon_0 \varepsilon_{AB}^v(\omega_1, \omega_2)\varepsilon_{AB}'^\mu(\omega_1, \omega_2, \hat{\mathbf{r}}_{12}) \times \tag{2}$$
$$\left\{ \left[\frac{\sigma_c}{r_{AB} - \sigma_{AB}(\omega_1, \omega_2, \hat{\mathbf{r}}_{12}) + \sigma_c} \right]^{12} - \left[\frac{\sigma_c}{r_{AB} - \sigma_{AB}(\omega_1, \omega_2, \hat{\mathbf{r}}_{12}) + \sigma_c} \right]^6 \right\}$$

where ω_1 and ω_2 are the molecular orientations, $\mathbf{r}_{AB} = r_{AB}\hat{\mathbf{r}}_{12} = \mathbf{r}_B - \mathbf{r}_A$ is the vector connecting the centres of sites A, B, $\sigma_{AB}(\omega_1, \omega_2, \hat{\mathbf{r}}_{12})$ is the anisotropic contact distance function, σ_c is the tunable well depth, $\varepsilon_{AB}^v(\omega_1, \omega_2)$ the interaction strength at zero separation and $\varepsilon_{AB}'^\mu(\omega_1, \omega_2, \hat{\mathbf{r}}_{12})$ the ad-hoc interaction term defined in [35], containing two empirical exponents μ and v, used for tuning the potential

angular dependence. The subscript A, B label the fullerene or mesogen particles. We refer to [34,35] for a complete description of the potential and the notation.

To model the fullerene sites interaction we have employed the Girifalco central potential [36], as fitted by a GB potential [28]. The parameterization of the R and D models are described in [28] and [37] respectively, while the mixing rules for computing heterogeneous interactions in [34]. The complete details of the particles employed in the simulations, are given in Table 1 and Table 2.

We performed a large number of MC experiments in the isobaric-isothermal (NPT) ensemble at dimensionless pressure $P^* = P\sigma_0^3/\varepsilon_0$ and temperature $T^* = T\sigma_0^3/\varepsilon_0$. Samples of N=500 fullerenic mesogens were studied. An isotropic condensed phase was prepared first. Simulations were then started from equilibrated configurations in the isotropic phase and subsequently performed in a cooling-down sequence of runs, each of them starting from the final equilibrated configuration obtained at the previous temperature. The length

of MC equilibration runs varied from 500 kcycles for generating the first isotropic configurations and up to 1,000 kcycles on the approach to the ordered phases at lower temperatures, each cycle corresponding to N attempted single-site MC moves. Typical acceptance ratio was 0.4. An orthogonal simulation box with periodic boundary conditions was used, with sides fluctuating independently during the MC evolution. During production runs thermodynamic observables have been accumulated for averaging and data analysis every 20 cycles.

The phase behavior has been detected from the temperature dependence of the average values of thermodynamic quantities like enthalpy $\langle H^* \rangle = \langle U^* \rangle + P^* \langle V^* \rangle$ and orientational order parameters, in particular the uniaxial order parameter $\langle P_2 \rangle = \langle 3(\hat{\mathbf{z}} \cdot \mathbf{n})^2 - 1 \rangle / 2$ showing the average orientational order of the molecular $\hat{\mathbf{z}}$ axis with respect to the liquid crystalline director $\mathbf{n}$, and the biaxial order parameter $\langle R_{22}^2 \rangle$ (see [38] for details of its computation).
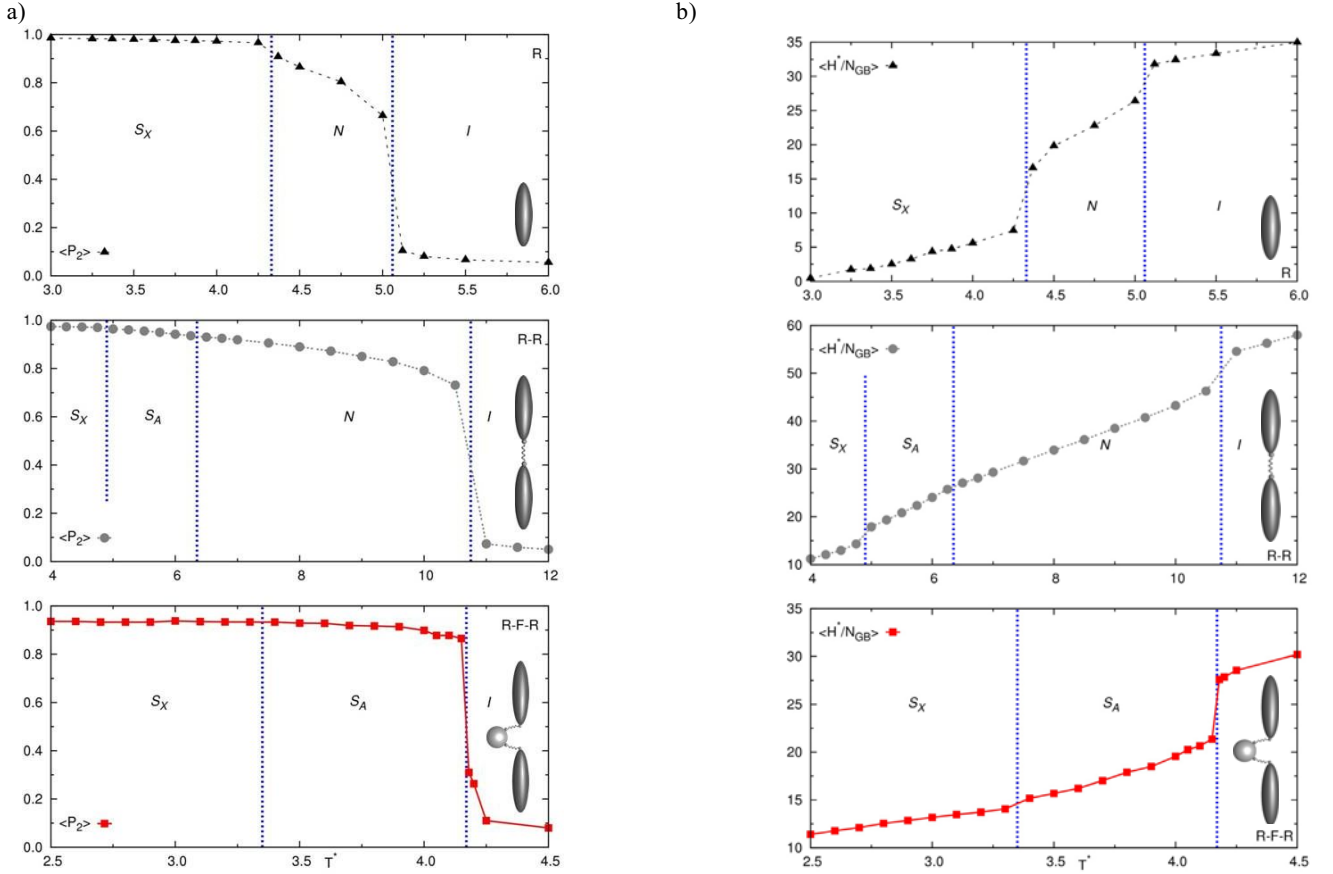
Fig. 3 Orientational order parameter $\langle P_2 \rangle$ (a), enthalpy per moiety $\langle H^*/N_{GB} \rangle$ (b) as a function of temperature T^*, for systems of N=1000 rod-monomers (model R, top); N=1000 rod-dimers (model R-R, middle); N=500 rod-fullerene derivatives (model R-F-R, bottom). Pressure is P^*=20.

Additional insight into the molecular organization adopted by these systems and in particular on the arrangement of the fullerenes and of the mesogenic units has been obtained computing pair correlation functions, referred to units U=F,R,D.

The radial correlation function $g_0(r)$ gives the probability to find a molecule at distance r if the other is at the origin of the coordinate system:

$$g_0^{UU}(r) = \frac{1}{4\pi r^2 \rho} \langle \delta(r - r_{ij}) \rangle_{ij} \tag{3}$$

Pair correlation functions perpendicular and parallel to the director **n**, are:

$$g_\perp^{UU}(r) = \frac{1}{2\pi R_\perp \rho} \langle \delta(r - |\mathbf{r}_{ij} \times \mathbf{n}|) \rangle_{ij} \tag{4}$$

$$g_\parallel^{UU}(r) = \frac{1}{2\pi R_\parallel \rho} \langle \delta(r - \mathbf{r}_{ij} \cdot \mathbf{n}) \rangle_{ij} \tag{5}$$

which give the probability to find a molecule respectively in a layer perpendicular to the director and in cylindrical shells having as axis the director ($R_\parallel$ and $R_\perp$ are the radii of the corresponding cylindrical sampling regions). All the two particles averages $\langle ... \rangle_{ij}$ are computed over all molecular pairs and configurations. The pair correlation functions parallel to the director are particularly useful for the identification of the layered structure of mesogens and fullerene units.

To help us to locate the phase transitions we have also calculated specific diffusion indicators $\Delta_\parallel$, $\Delta_\perp$, $\Delta_{iso}=(\Delta_\parallel+2\Delta_\perp)/3$, obtained directly from the slope of the mean square displacements of particle positions along different directions, vs. the number of cycles τ:

$$\Delta_i = \frac{1}{\tau} \langle (r_i(\tau) - r_i(0))^2 \rangle \; ; \tag{6}$$

where we have used τ=200 kcycles.

III Results: rod-like mesogenic fullerene derivatives

The temperature dependence of the average enthalpy and orientational order parameter for the systems of rod-fullerene derivatives, at pressure $P^*=20$, is shown in Fig. 3 in comparison with the corresponding phase behaviour of two systems containing the same mesogen unit: N=1000 monomeric-rod mesogens (system R) and N=1000 rod-dimers (system R-R) with spacer length (-) equal to $0.1\sigma_0$. In particular, our aim is to find out to which extent, in the presence of fullerene units, the mesogens still retain their self-assembling properties.

Starting from the monomeric rod system (model R) we recall first that the "standard" GB system with $\sigma_\parallel/\sigma_\perp=3$, $\varepsilon_\parallel/\varepsilon_\perp = 0.2$,

$\mu=1$, $\nu=3$ has on cooling the sequence isotropic (I), nematic (N), smectic (S), crystalline smectic (S_X) phases [30]. The same sequence is observed here even if the parameters (e.g. $\sigma_\parallel/\sigma_\perp= 3.71$) and the thermodynamic conditions are different (here $P^*=20$) and consequently the transition temperatures do not coincide. Moving to the R-R system we see that the main effect is the stabilization of the nematic phases and the appearance of a smectic A phase. Introducing the central fullerene unit (system R-F-R) has a more drastic effect. Particularly remarkable are the suppression of the nematic phase, present both in R and R-R systems and the lowering of the clearing temperature.

a)

b)
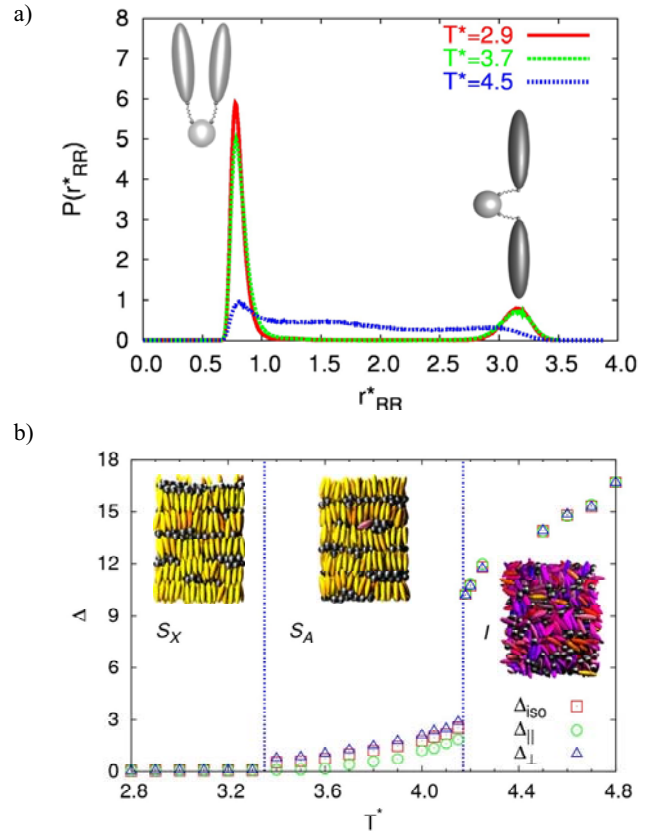
Fig. 4 a) Probability distribution of the intramolecular mesogen-mesogen separation (r^*_{RR}), showing the two peaks associated to the bent and linear molecular shapes. b) Temperature dependence of the parallel ($\Delta_\parallel$) and perpendicular ($\Delta_\perp$) diffusion indicators are shown, together with the average ($\Delta_{iso}= (\Delta_\parallel+2\Delta_\perp)/3$). In the insets, snapshots of molecular assemblies for R-F-R derivatives in Crystal (S_X), Smectic A (S_A) and Isotropic (I) phase. The fullerene moiety is represented as a black sphere, the GB mesogens are colour coded according to their orientation respectively to the phase director (yellow for parallel orientation, blue for orthogonal).
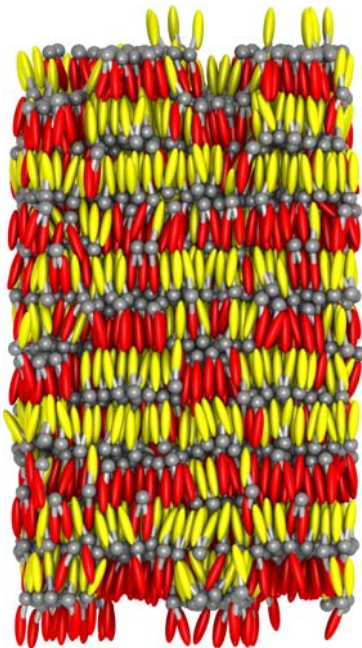
The order parameter $\langle P_2 \rangle$ reaches high values immediately after the transition I-S_A and is then nearly constant throughout the temperature range of the solid/smectic phases. It comes out that C60, rather than being just disruptive on any type of ordering, favours instead positional structuring, promoting smectic rather then nematic.
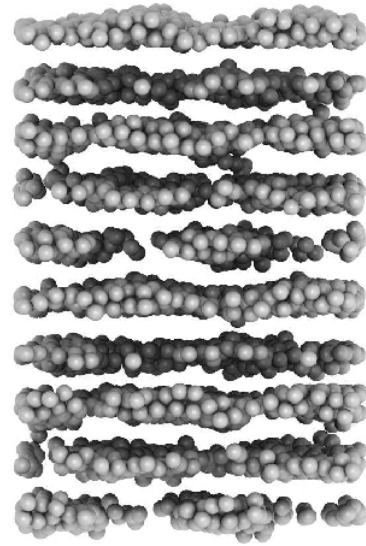
a)
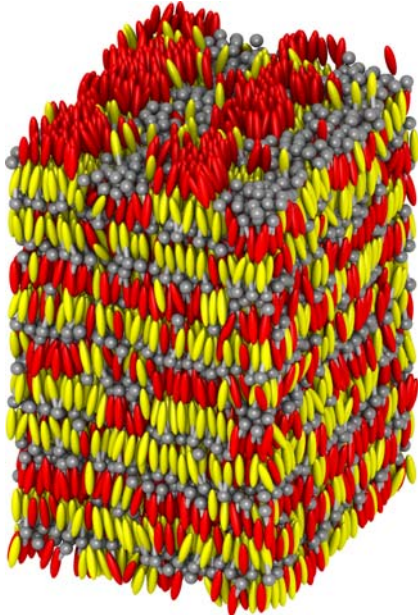
b)

c)

Fig. 5 Snapshot of a molecular assembly of N=4000 R-F-R derivatives at T^*=3.7 in the smectic A phase (oblique and frontal view in plates a and b). The rod units are colour coded on the basis of the alignment of the rod-fullerene bond with respect to the layer normal: yellow if they are parallel oriented, red if antiparallel. The rod-fullerene bond vectors are rendered with arrows. A nearly two-dimensional segregation of the fullerene spheres is evident. To help in the visualization only the spherical particles have been represented in plate c.

The internal flexibility appears as an essential feature for the self-assembly properties of the mesogenic-fullerene derivatives. In fact, in comparison with the rigid model proposed in [28], the nematic phase disappears, resulting in a direct isotropic-smectic transition, in agreement with the experimental evidences for the majority of compounds of this class [22,29]. In addition, the flexible model shows a reduction on the variation of the density on going from isotropic to smectic.

The molecular flexibility of the proposed R-F-R model has been monitored through the probability distribution $P(r^*_{RR})$ of the intramolecular mesogen-mesogen separation r^*_{RR} (Fig. 4a). Quite interestingly, at low temperature (S_X and S_A phase), the peak at $r^*_{RR} \approx 0.7$ (corresponding to folded conformation of R sites) is 6 times higher than the the one at $r^*_{RR} \approx 3.2$, showing that molecules prefer to adopt a bent ("U"-like) shape rather than a linear one.

We noticed that although the slopes of mean square molecular displacements in the different directions $\Delta_{||}$, $\Delta_{\perp}$, exhihibit a significant decrease across the ordering transition, there still exist a non negligible mobility in the smectic, particularly in the layer planes ($\Delta_{\perp}$ in Fig. 4b).

Snapshots of typical molecular organizations obtained from simulations at selected temperatures are given in the insets in Fig. 4b. In the smectic phase, we observe an interesting microsegregation of fullerene spheres in discontinuous layers.

This self-organizing feature is particular striking, so to validate it we have simulated a significantly larger sample with N=4000 fullerenic molecules at the smectic temperature T^*=3.7 (see Fig. 5) confirming that the same type of organization is formed.

a)

b)

c)
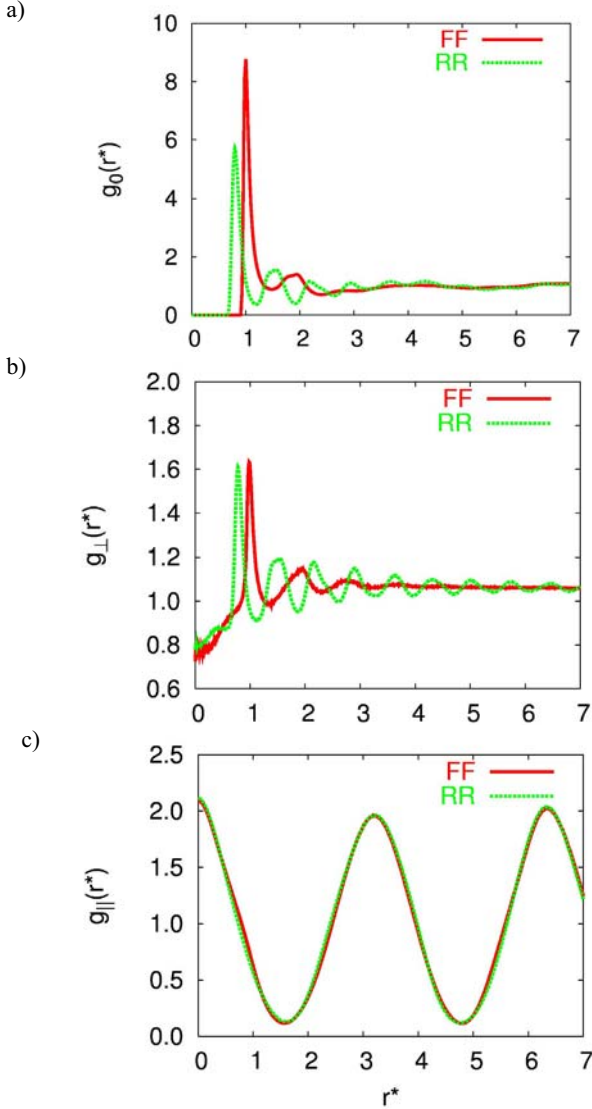
Fig. 6 Correlation functions $g_0(r^*)$ (plate a), $g_\perp(r^*)$ (plate b), $g_\parallel(r^*)$ (plate c), for both fullerene (FF) and rod (RR) sites for a system of N=4000 R-F-R molecules at T^*=3.7 (Smectic A).

The structural features become apparent and can be quantified in the pair distribution functions (Fig. 6); in particular the onset of a smectic phase with microsegregation of both F and R sites is indicated by the oscillations in the longitudinal correlation functions $g_\parallel^{RR}(r)$ and $g_\parallel^{FF}(r)$. These show their maxima separated by a distance equal to $r^* \approx 3.0$, which roughly corresponds to the length of the molecule in the U-like conformation and to half of the length for the linear conformation.

From correlation functions $g_\perp^{FF}(r)$ and $g_\perp^{RR}(r)$ (Fig. 6) it can be noticed that in the smectic layer the rod mesogens are more correlated than the spherical sites of the molecules. The rapid decay of the density correlation for the fullerene sites in the smectic phase and the absence of the characteristic splitting of the second peak of the curves, highlight the lack of long range positional and of hexagonal order and the liquid-like order inside the layers.

IV Results: disc-like mesogenic fullerene derivatives

We now turn to the discotic based mesogen system, that to our knowledge, has not been previously studied for neither rigid nor flexible molecular models. In analogy with the rod case, the temperature dependence of enthalpy and orientational order parameters of a systems of N=500 disc-fullerene derivatives, have been investigated in relation to the corresponding phase behaviour of N=1000 monomeric-disc mesogens (system D) and N=1000 disc-dimers (system D-D) with spacer length equal to $0.2\sigma_0$ (cf. references [37] and [33] for detailed investigations of D and D-D systems). All the simulations were run at P^*=3.5 and at different temperatures T^* in steps of 0.2 or less (Fig. 7).

Starting again from the monomeric system (model D) we observe upon cooling the sequence isotropic (I), nematic discotic (N_D), then columnar hexagonal (Col_h), and crystal (Col_X). Dimerization has for this disc-based system the effect of strongly stabilizing the N phase (T^*_{NI} goes from 1.15 to 3.35), while the formation of the hexagonal columnar phase occurs roughly at the same T^* than the monomer, giving rise to a huge widening of the nematic interval.

The D-F-D model yields mesomorphism with isotropic, nematic, biaxial columnar and crystalline phase (see also Fig. 8). Comparing with both D and D-D models we observe a reduction of the nematic range and of the order parameter $\langle P_2 \rangle$ in the nematic phase.

Concerning the fullerenes organization at low temperature, it is evident (see the snapshots in Fig. 8 and 9) the tendency of the fullerene moieties to organize in walls (two dimensional segregation) rather than in columns.
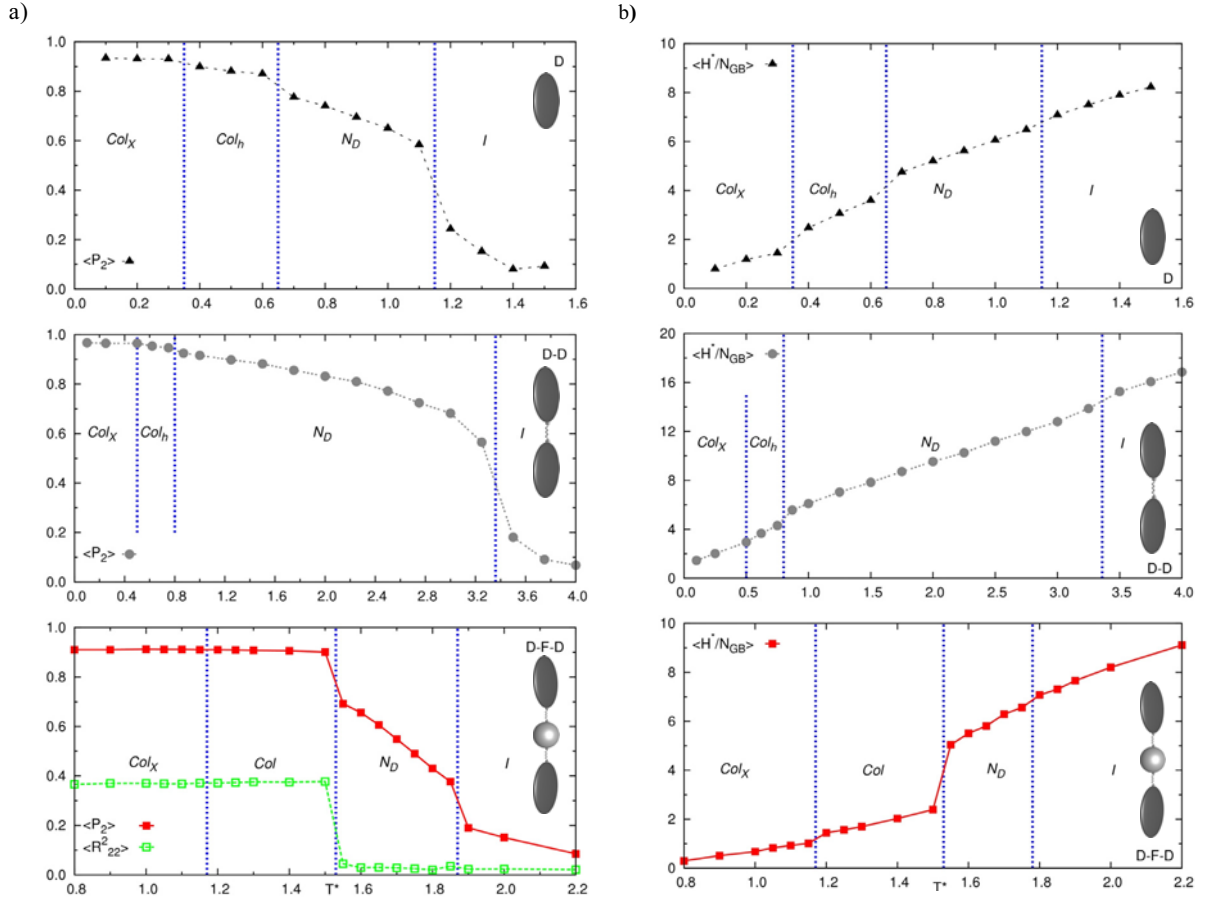
Fig. 7 Orientational order parameter $\langle P_2 \rangle$ (a), enthalpy per moiety $\langle H^*/N_{GB} \rangle$ (b) as a function of temperature T^*, for systems of $N=1000$ disc-monomers (model D, top); $N=1000$ disc-dimers (model D-D, middle); $N=500$ disc-fullerene derivatives (model D-F-D, bottom). Pressure is $P^*=3.5$.

The structural characterization of the phase is achieved by separate simulation of a sample of $N=4000$ molecules at $T^*=1.25$, calculating the radial distribution for both discotic, $g_0^{DD}(r)$ and fullerenic $g_0^{FF}(r)$ sites. From Fig. 10 we notice that the fullerene spheres subsystem is much more structured for the discotic than the rod-based case (Fig. 6).

It is interesting to compare the different fullerene aggregation patterns given by different mesogens (rod and disc) at low temperature. In the case of calamitic mesogens (Fig.11a) we observe layers of fullerenes which do not span the whole available box space. The layers, with variable thickness of 1-2 fullerenes on average, have their plane normal **k** parallel to the nematic director **n**.

The discotic based system (Fig. 11b), on the other hand, presents much more regular C60 layers of one fullerene unit of thickness, extending through all the sample. Remarkably, the plane normals **k** are oriented perpendicular to the columnar director **n**, leading to a biaxial phase as shown by the $\langle R_{22}^2 \rangle$ order parameter in Fig. 7. To maximize the packing the long axes of the D-F-D molecules are tilted of an angle $\theta=20°$ with respect to **k**, and the discs belonging to the same molecules are often not coplanar.
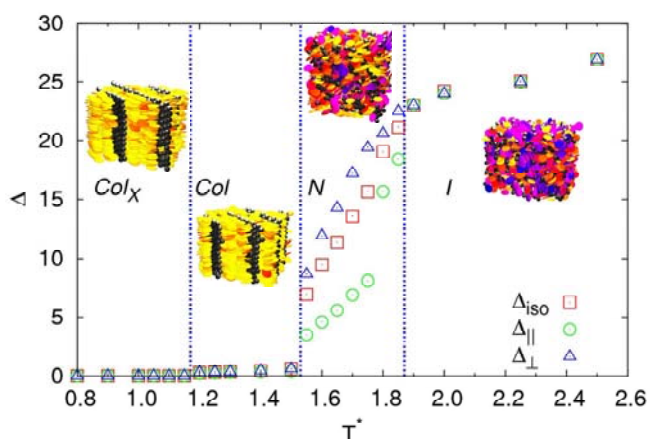
Fig. 8 Temperature dependence of the parallel ($\Delta_{\parallel}$) and perpendicular ($\Delta_{\perp}$) diffusion indicators are shown, together with
5 the average ($\Delta_{iso}= (\Delta_{\parallel}+2\Delta_{\perp})/3$) (plate a). In the inset, snapshots of molecular assemblies for D-F-D derivatives in Crystal (Col$_X$), Columnar (Col), Nematic (N) and Isotropic (I) phase. The fullerene moiety is represented as a black sphere, the GB mesogens are colour coded according to their orientation respectively to the phase
10 director.

These phase organisations can be rationalised by the
15 combination of two effects; on one hand the strong interaction between fullerenes induces their microsegregation, on the other the mesogens tend to arrange preferentially in one direction, and the dimerization appears to drive also the directionality of C60 aggregation.
20 In the R-F-R case, the mesogens alignment direction is parallel to the long molecular axis (where the C60 lies), hence in the smectic phase the layer normal is parallel to **n**, while on the contrary in the D-F-D case the mesogens alignining direction is perpendicular to the molecular axis: consequently
25 the layer normal and the director of the columnar phase lay perpendicular. It is likely that less symmetric variations of the position of the C60 with respect to the two mesogens would induce even more exotic organisations.

30

Conclusions

We have studied, by means of Monte Carlo simulations, the molecular organisations obtained from two symmetric mesogen-C60-mesogen systems, where the mesogens have
35 respectively rod or disc shape and are flexibly attached to the fullerene sphere.
For calamitic fullerene derivatives the simulations show that upon lowering the temperature molecules arrange in smectic layers where fullerene spheres and mesogenic rods are
40 microsegregated [21], leading to an interesting quasi planar system of fullerenes.

a)

b)

c)
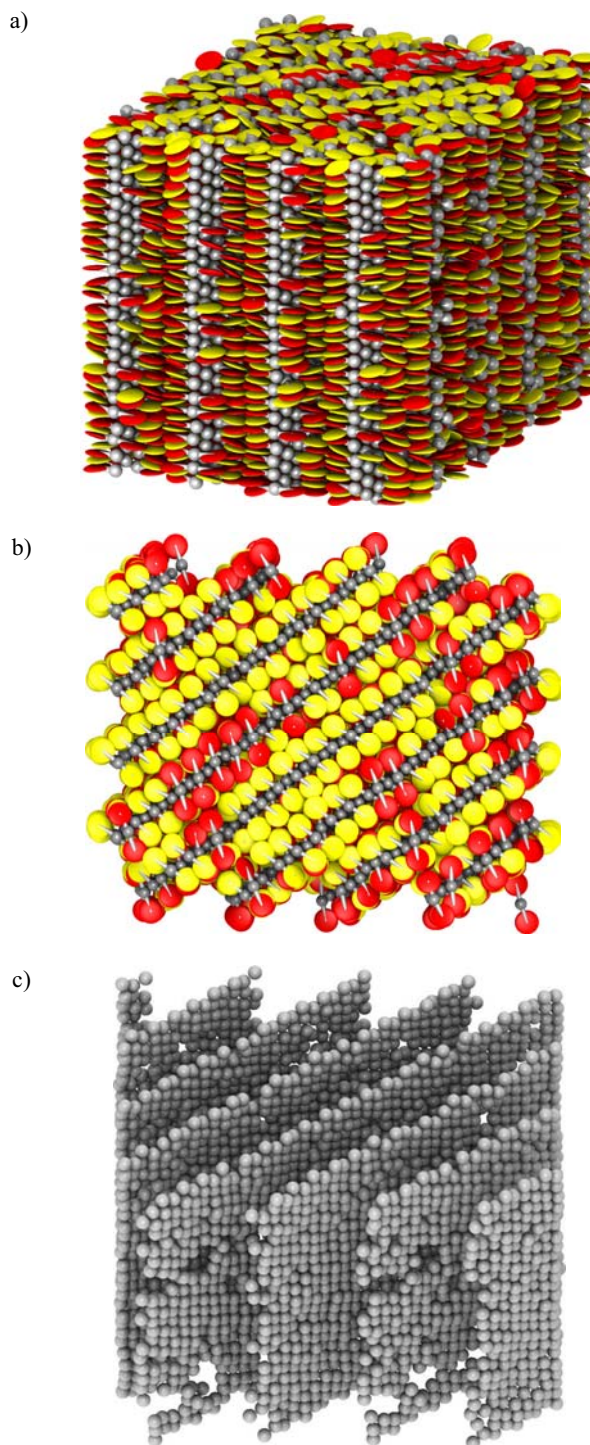
Fig. 9 Snapshots for the system of N=4000 D-F-D molecules at
45 T^*=1.25 (Columnar phase), oblique (plate a) and top (plates b) views. The discs units are colour coded depending on the in plane alignment of the disc-fullerene bond vectors (rendered with arrows) along two axes: the layer normal (**k**) and the vector product of the director and the layer normal (**k**×**n**). In particular, if the scalar
50 product of the bond vector with both axes is positive the disc gets colored red, otherwise yellow. In (c), to help in the visualization of the layers only the fullerenes have been represented.

a)

b)

c)
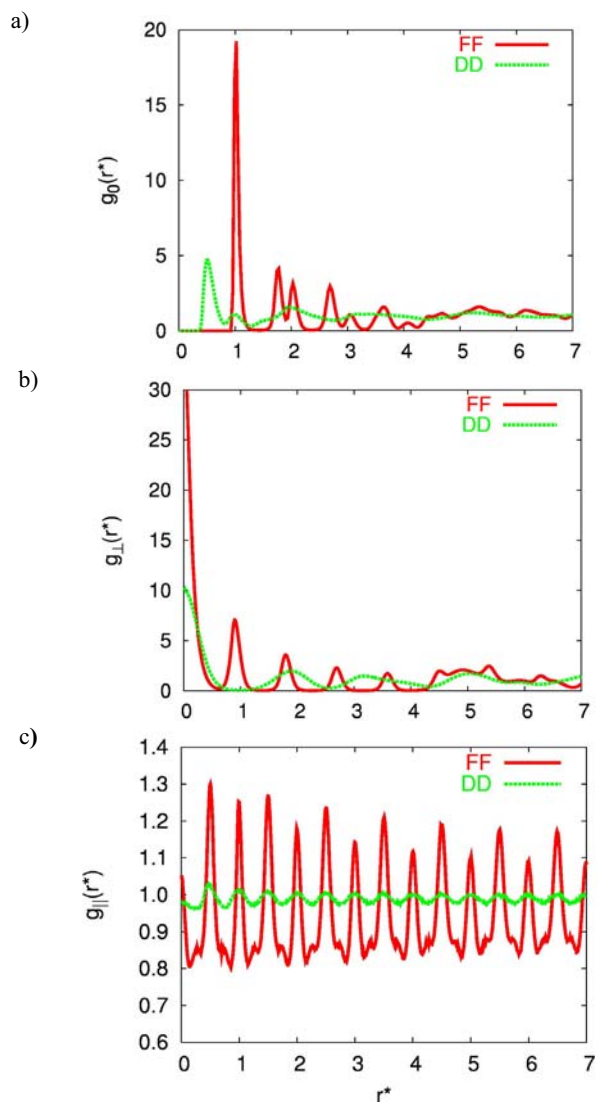
Fig. 10 Correlation functions $g_0(r^*)$ (plate a), $g_\perp(r^*)$ (plate b), $g_\parallel(r^*)$ (plate c) for both fullerene (FF) and discotic (DD) sites for a sytem of N=4000 D-F-D molecules at T^*=1.25 (Columnar).

5

For discotic fullerene derivatives the model yields mesomorphism with isotropic, nematic and columnar phases. Also in this case, at low temperature, a two-dimensional microsegregation of fullerenes is apparent. Remarkably, in
10 this D-F-D system the fullerenes "walls" are well formed with fullerenes closely packed, differently from R-F-R case in which layers present ample regions of discontinuity.
The predicted phase organisations, particularly for the discotic fullerene mesogenic case, seem very promising in
15 terms of optimization of electronic properties and we hope that this modeling work will stimulate the synthesis of these novel materials.

a)

b)
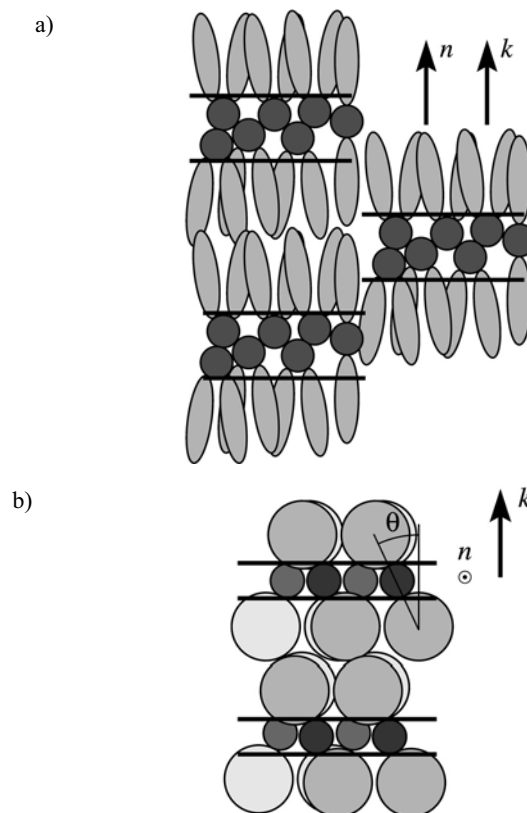
Fig. 11 Sketches of the local fullerene-mesogen arrangement for
20 R-F-R (a) and D-F-D (b) systems showing the features of the segregation of fullerene sites, the relative orientation between the phase director **n** and the layer normal **k** and, for the D-F-D model, the tilt angle θ between the bond vectors and **k**.

25

Acknowledgements

35 ## Notes and references

*aDipartimento di Chimica Fisica ed Inorganica, Università di Bologna and INSTM-CRIMSON, Viale Risorgimento 4, IT-40136 Bologna, Italy Fax: +39 051 6447012; Tel: +39 051 6447012;
E-mail:Claudio.Zannoni@unibo.it.See DOI: 10.1039/b000000x/*
40

1 M. Kitamura, S. Aomori, J. H. Na and Y. Arakawa, *Appl. Phys. Lett.*, 2008, **93**, 033313.

45 2 J. N. Haddock, X. H. Zhang, B. Domercq and B. Kippelen, *Org. Electronics*, 2005, **6**, 182.

3 A. Opitz, M. Bronner and W. Bruetting, *J. Appl. Phys*., 2007, **101**, 063709.

4 H. Hoppe and N. S. Sariciftci, *J. Mat. Res.*, 2004, **19**, 1924.

5 J. L. Segura, N. Martin and D. M. Guldi, *Chem. Soc. Rev.*, 2005, **34**, 31.

6 S. Gunes, H. Neugebauer and N. S. Sariciftci, *Chem. Rev.*, 2007, **107**, 1324.

7 D. M. Guldi, *Chem. Comm.*, 2000, 321.

8 M. Hallermann, S. Haneder, E. Da Como, *Appl. Phys. Lett*., 2008, **93**, 053307.

9 T. Chuard and R. Deschenaux, *Helv. Chim. Acta*, 1996, **79**, 736.

10 D. Gebeyehu, C. J. Brabec, F. Padinger, T. Fromherz, J. C. Hummelen, D. Badt, H. Schindler and N. S. Sariciftci, *Synth. Met.*, 2001, **118**, 1.

11 Y. Kim, S. Cook, S. M. Tuladhar, S. A. Choulis, J. Nelson, J. R. Durrant, D. D. C. Bradley, M. Giles, I. McCulloch, C.-S. Ha and M. Ree, *Nat. Mater.*, 2006, **5**, 197.

12 S. Yoo S, B. Domercq and B. Kippelen, *Appl. Phys. Lett*., 2004, **85**, 5427.

13 J. Gilot, M. M. Wienk, R. A. J. Janssen, *Appl. Phys. Lett*., 2007, **90**, 143512.

14 G. Hadziioannou, *MRS Bull*., 2002, **27**, 456.

15 M. Granstroem, K. Petritsch, A. C. Arias, A. Lux, M. R. Andersson and R. H. Friend, *Nature*, 1998, **395**, 257.

16 M. C. Abramo, C. Caccamo, D. Costa, G. Pellacane and R. Ruberto, *Phys. Rev. E*, 2004, **69**, 031112.

17 J. C. Hummelen, B. W. Knight, F. Lepeq, F. Wudl, J. Yao and C. L. Wilkins, *J. Org. Chem.*, 1995, **60**, 532.

18 N. S. Sariciftci, L. Smilowitz, A. J. Heeger and F. Wudl, *Science*, 1992, **258**, 1474.

19 A. Cravino, *Polym. Int.*, 2007, **56**, 943.

20 N. Tirelli, F. Cardullo, T. Habicher, U. W. Suter and F. Diederich, *J. Chem. Soc.-Perkin Trans.*, 2000, **2**,193.

21 M. Sawamura, K. Kawai, Y. Matsuo, K. Kanie, T. Kato and E. Nakamura, *Nature*, 2002, **419**, 702.

22 M. Manickam, A. Smith, M. Belloni, E. J. Shelley, P. R. Ashton, N. Spencer and J. A. Preece, *Liq. Cryst*., 2002, **29**, 497.

23 R. Deschenaux, B. Donnio and D. Guillon, *New J. Chem*., 2007, **31**, 1064.

24 T. I. Hukka, T. Toivonen, E. Hennebicq, J-L. Brédas, R. A. J. Janssen and D. Beljonne, *Adv. Mater*, 2006, **18**, 1301; D. Cheyns, H. Gommans, M. Odijk, J. Poortmans, P. Heremans, *Solar Energy Materials & Solar Cells*, 2007, **91**, 399.

25 Y. Shimizu, K. Oikawa, K. Nakayama and D. Guillon, *J. Mater. Chem.*, 2007, **17**, 4223.

26 G. Cinacchi, *Chem. Phys. Lett*. 2004, **395**, 335.

27 (a) S. D. Peroukidis, A. G. Vanakaras and D. J. Photinos, *J. Chem. Phys*., 2005, **123**, 164904; (b) S. D. Peroukidis A. G. Vanakaras and D. J. Photinos, *Soft Matter*, 2008, **4**, 493.

28 A. Sazonovas, S. Orlandi, M. Ricci, C. Zannoni and E. Gorecka, *Chem. Phys. Lett*., 2006, **430**, 297.

29 B. Dardel, D. Guillon, B. Heinrich and R. Deschenaux, *J. Mater. Chem.,* 2001, **11**, 2814.

30 R. Berardi, A. P. J. Emerson and C. Zannoni, *J. Chem. Soc. Faraday Trans.*, 1993, **89**, 4069.

31 C. Zannoni, *J. Mater. Chem.*, 2001, **11**, 2637.

32 R. Berardi, D. Micheletti, L. Muccioli, M. Ricci and C. Zannoni, *J. Chem. Phys*., 2004, **121**, 9123.

33 I. Miglioli, L. Muccioli, S. Orlandi, M. Ricci, R. Berardi, C. Zannoni, *Theor. Chem. Acc.,* 2007, **118,** 203.

34 R. Berardi, C. Fava and C. Zannoni, *Chem. Phys. Lett.*, 1998, **297**, 8.

35 R. Berardi, C. Fava and C. Zannoni, *Chem. Phys. Lett*., 1995, **236**, 462

36 (a) L. A. Girifalco, *J. Phys. Chem.,* **95**, 5370 (1991); (b) L. A. Girifalco, *J. Phys. Chem.*, 1992, **96**, 858.

37 S. Orlandi, L. Muccioli, M. Ricci and C. Zannoni, *Chem. Central J.,* 2007, **1**, 15.

38 R. Berardi, L. Muccioli, S. Orlandi, M. Ricci, C. Zannoni**,** *J. Phys.: Condens. Matter*, 2008, **20**, 463101.

39 R. J. Bushby, I. W. Hamley, Q. Y. Liu, O. R. Lozman and J. E. Lydon, *J. Mater. Chem*., 2005, **15**, 4429.